IRAQI JOURNAL OF APPLIED PHYSICS
Vol. 22, No. 2, April-June 2026, pp. 153-158

Haneen H. Shaaban
Mohammed A. Hameed*

Department of Physics,
College of Science,
University of Baghdad,
Baghdad, IRAQ
* Corresponding author email:
mohammed.a@sc.uobaghdad.edu.iq

Optoelectronic Characteristics of Al_2O_3/Si Multilayer Structures Fabricated by DC Reactive Sputtering Technique

In this work, optoelectronic characteristics of Al_2O_3/Si multilayer structures were presented and analyzed. These structures were prepared by dc reactive sputtering technique with different thicknesses of Al_2O_3 layer (200, 250, and 325 nm). The 200-nm sample showed the highest current levels. The samples with 200 and 250 nm thickness exhibit a much more pronounced photoresponse, while the 325-nm sample shows a higher dark current to begin with. Similarly, the same samples (200 and 250 nm) show remarkably similar behaviors of spectral responsivity (R_λ), both peaking around 0.38 A/W in the NIR region (800-850 nm), while their responsivity is relatively low in the visible range (400-700 nm), but shows a sharp increase beyond 750 nm. This suggests that for these deposition times, the Al_2O_3 layer allows for effective photon absorption in the Si substrate at longer wavelengths. In contrast, the 300-nm sample exhibits significantly lower responsivity values, with the peak responsivity reaching 0.0038 A/W. This drop in responsivity indicates that the thicker Al_2O_3 layer impedes the photo-generation and collection of carriers. The behaviors of the external quantum efficiency (EQE) and specific detectivity (D^*) were similar to that of the spectral responsivity. The EQE was peaking at ~55-56% around 850 nm, while the specific detectivity was peaking at approximately 0.55×10^{12} Jones around 850 nm for both 200 and 250-nm samples.

Keyword: Alumina; DC sputtering; Multilayer structures; Optoelectronics
Received: 23 May 2025; Revised: 20 July 2025; Accepted: 27 July 2025

1. Introduction

Multilayer structures fabricated from nanostructures on silicon substrates are critical in numerous practical applications, particularly in microelectronics and optoelectronics [1-3]. Silicon, being a mature and widely used semiconductor, provides a robust platform for integrating various functional layers [4,5]. By depositing nanoscale layers of different materials, such as oxides, nitrides, or metals, precise control over the overall device characteristics can be achieved. These multilayer stacks enable functionalities like enhanced light absorption or reflection, improved electrical insulation, optimized charge transport, and superior protection against environmental degradation. Examples include advanced gate stacks in transistors for higher performance, anti-reflection coatings on silicon solar cells for increased efficiency, and complex optical filters for sensing applications [6-10]. The ability to engineer properties at the nanoscale within these multilayer architectures is fundamental to the continued advancement of high-performance electronic and photonic devices [11-15].

Aluminum oxide (Al_2O_3), commonly known as alumina, is a material with diverse applications due to its excellent optical, electrical, and mechanical properties [16-18]. In nanostructured forms, Al_2O_3 exhibits enhanced characteristics suitable for various fields, including optoelectronics [19,20]. Preparation methods for Al_2O_3 nanostructures include techniques like pulsed-laser deposition (PLD), atomic layer deposition (ALD), chemical vapor deposition (CVD), and reactive sputtering [21-24]. For optoelectronic applications, Al_2O_3 thin films are valued for their high transparency across a wide spectral range, high dielectric constant, and good insulating properties. These characteristics make them ideal for use as gate dielectrics in thin-film transistors, passivation layers in solar cells, and protective coatings for optical components [25,26]. Their stability and tunable refractive index also contribute to their importance in fabricating anti-reflection coatings and waveguides in integrated optical devices [27,28].

DC reactive magnetron sputtering is a versatile and reliable technique for preparing thin films, including nanostructured Al_2O_3. This method involves introducing a reactive gas, such as oxygen, which reacts with the sputtered target material to form a compound film [29-32]. A key advantage of DC reactive sputtering lies in its ability to precisely control the film's properties by optimizing parameters like oxygen partial pressure, DC power, working gas pressure, and substrate temperature [33,34]. This fine control is particularly beneficial for fabricating multilayer structures, where distinct layers with tailored compositions and properties are required [35]. By sequentially depositing different materials or varying reactive gas compositions, sophisticated multilayer stacks can be achieved, enabling the creation of advanced devices with enhanced functionalities [36].

The technique allows for the deposition of a wide variety of compounds, offering broad applicability [37,38].

2. Experimental Part

A dc reactive sputtering system was used to deposit Al_2O_3 thin films on silicon substrates with different thicknesses. The film thickness was determined by the deposition time of the Al_2O_3 layer. A highly-pure (99.99%) target of aluminum was sputtered in presence of oxygen with mixing ratio of 50:50 with argon in the gas mixture. The target and silicon substrates were thoroughly cleaned and dried before the deposition process. The target was maintained carefully on the cathode and the deposition chamber was initially evacuated to 0.001 Torr. The plasma column was generated by electrical discharge of argon as a high dc voltage (up to 5 kV) was applied between the electrodes. The deposition process was carried out at room temperature, the discharge voltage during operation was 650-700 V, and the discharge current was kept at 25 mA. The deposition times were 60, 90 and 120 min. and the inter-electrode distance was 4 cm. The optimum discharge current was determined according to the stability of the discharge plasma and the pressure of gas mixture was about 0.15 mbar. The flow rate of the gas mixture into the deposition chamber could be precisely controlled, and the temperature inside the chamber was measured by a precision thermometer. The gas mixer was supplied with argon and oxygen gases from gas cylinders and the mixing ratio was controlled by fine needle valves. More details on this sputtering system can be found elsewhere [39-42]. The film thickness measurements were carried out using the optical interferometry method. This method is based on the interference of a coherent light beam reflected from a thin film surface and substrate bottom, with error rate of about 3%. A 630nm diode laser was used as a light source and the film thickness was determined using the following formula:

$$d = \frac{\Delta x}{x} \cdot \frac{\lambda}{2} \qquad (1)$$

where x is the fringe width, Δx is the distance between two adjacent fringes, and λ is the laser wavelength

The electrical and optoelectronics characteristics were determined throughout the current-voltage characteristics, photocurrent as a function of applied reverse voltage, spectral responsivity, external quantum efficiency, and specific detectivity.

3. Results and Discussion

Figure (1) illustrates the current-voltage (I-V) characteristics of the Al_2O_3/Si structures prepared with different thicknesses of the Al_2O_3 layer (200, 250, 325 nm). A clear trend emerges as the deposition time, and presumably the film thickness, increases. Figure (1a) shows the highest current levels, reaching approximately 190 μA in forward bias at 5V and about −120 μA in reverse bias at -5V. As the Al_2O_3 layer thickness was increased to 250 nm, (Fig. 1b), the current significantly decreases, with forward current reaching only about 40 μA and reverse current around −7 μA at 5V and -5V respectively. The most dramatic reduction in current is observed in Fig. (1c), where the current levels are substantially lower, peaking at just over 10 μA in forward bias and remaining very close to zero in reverse bias. This progressive decrease in current with increasing Al_2O_3 layer thickness suggests that thicker Al_2O_3 layers act as more effective insulating barriers, reducing leakage current and enhancing the rectifying behavior of the Al_2O_3/Si junction. The transition from a more resistive behavior at 200 nm to a more insulating behavior at 325 nm highlights the crucial role of Al_2O_3 film thickness in controlling the electrical properties of these heterostructures.

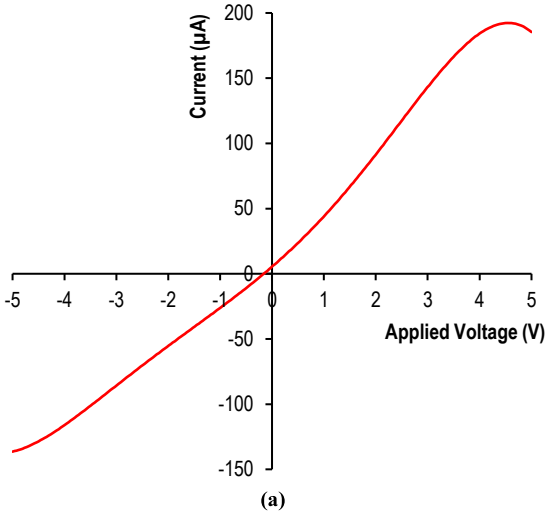

(a)

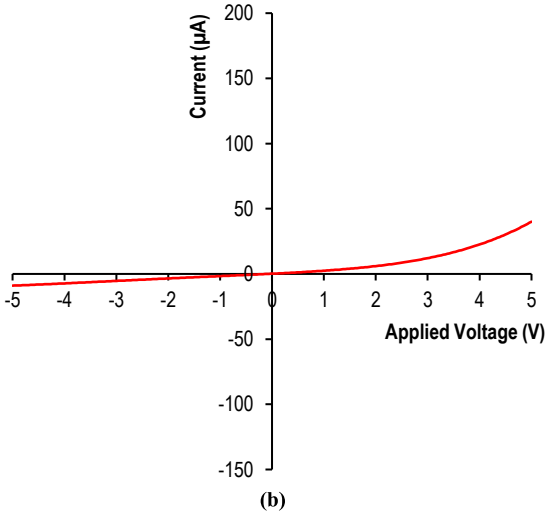

(b)

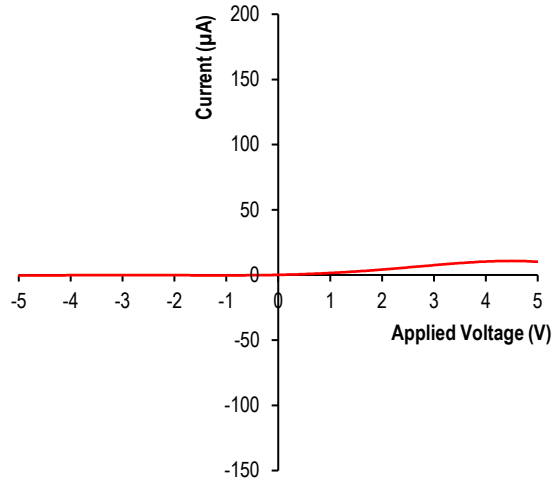

(c)

Fig. (1) The I-V characteristics of the Al_2O_3/Si structures prepared with different thicknesses of Al_2O_3 layer (a) 200nm, (b) 250nm, and (c) 325nm

Figure (2) illustrates the photocurrent response of the prepared Al_2O_3/Si structures under both dark and illuminated conditions. It displays the photocurrent (μA) as a function of reverse voltage (V). In Fig. (2a), under dark conditions, the photocurrent remains very close to zero, reaching approximately −10 μA at -5V. Upon illumination, the photocurrent significantly increases, reaching approximately −60 μA at -5V. Figure (2b) shows a similar trend but with significantly lower current magnitudes. Under dark conditions, the photocurrent is nearly zero, reaching about −0.4 μA at -5V. With illumination, the photocurrent increases, reaching around −1.1 μA at -5V. Figure (2c) presents a different behavior compared to the first two. Here, the dark current is more substantial, reaching approximately −135 μA at -5.5V. Under illumination, the photocurrent is higher than the dark current, but the difference between the two curves appears less pronounced in terms of relative increase compared to the first two figures, reaching about −105 μA at -5.5V.

Comparing the three figures, there's a clear variation in the scale of the photocurrent, which suggests differences in the device's photosensitivity or characteristics across samples. The samples of 200 and 250nm Al_2O_3 layer thickness exhibit a much more pronounced photoresponse, where illumination leads to a significant increase in current from a near-zero dark current. In contrast, the sample with 325nm Al_2O_3 layer thickness shows a higher dark current to begin with, and while illumination still increases the current, the overall shape and magnitude of the curves indicate distinct electrical properties, possibly due to variations in material properties or device architecture.

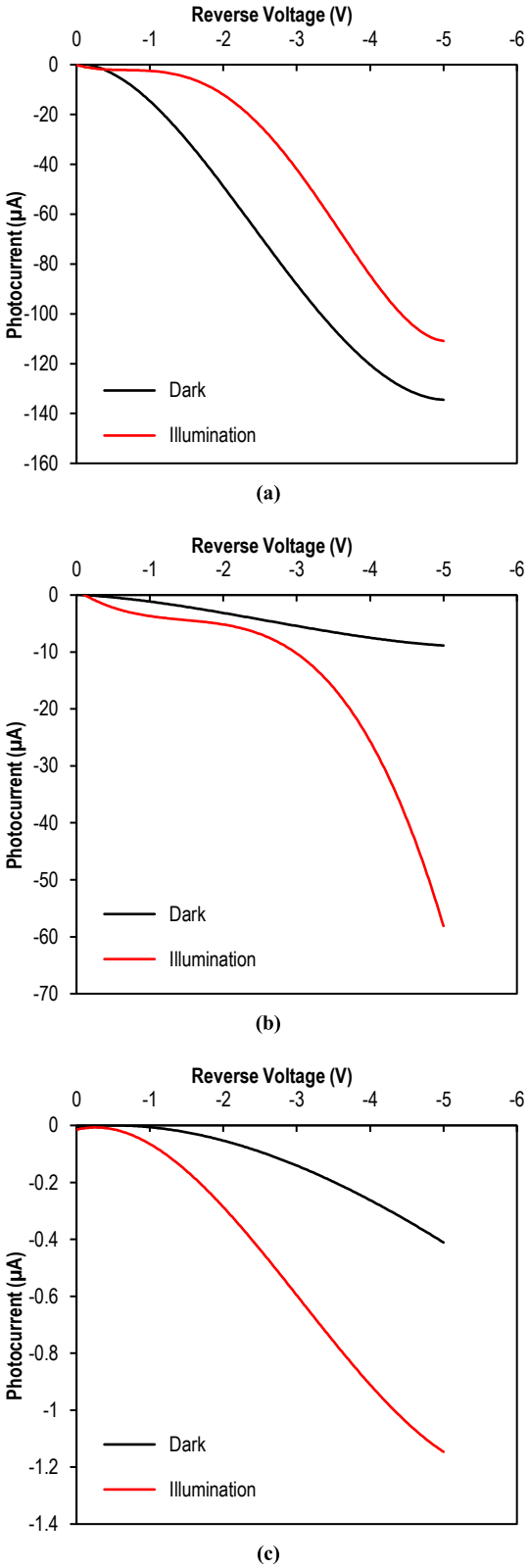

Fig. (2) The variation of photocurrent with applied reverse voltage in dark and under illumination for the Al_2O_3/Si structures prepared with different thicknesses of Al_2O_3 layer (a) 200nm, (b) 250nm, and (c) 325nm

Figure (3) illustrates the spectral responsivity as a function of wavelength for the Al_2O_3/Si structures with

varying Al_2O_3 layer thickness. A striking difference in responsivity magnitude is immediately apparent across the samples. The samples with 200 and 250nm thicknesses show remarkably similar responsivity curves, both peaking around 0.38 A/W in the near-infrared region (approximately 800-850 nm). Their responsivity is relatively low in the visible range (400-700 nm), typically below 0.15 A/W, but shows a sharp increase beyond 750 nm. This suggests that for this thickness range, the Al_2O_3 layer allows for effective photon absorption in the silicon substrate at longer wavelengths. In stark contrast, the sample with 325 nm Al_2O_3 layer exhibits significantly lower responsivity values, with the peak responsivity barely reaching 0.0038 A/W (or 3.8 mA/W). This substantial drop in responsivity for the 325nm sample indicates that the thicker Al_2O_3 layer, while potentially improving insulation as seen in previous I-V curves, severely impedes the photogeneration and collection of carriers. This could be due to increased absorption within the Al_2O_3 layer itself, a higher density of defects at the interface, or a greater barrier to carrier transport, thus limiting the device's performance as a photodetector.

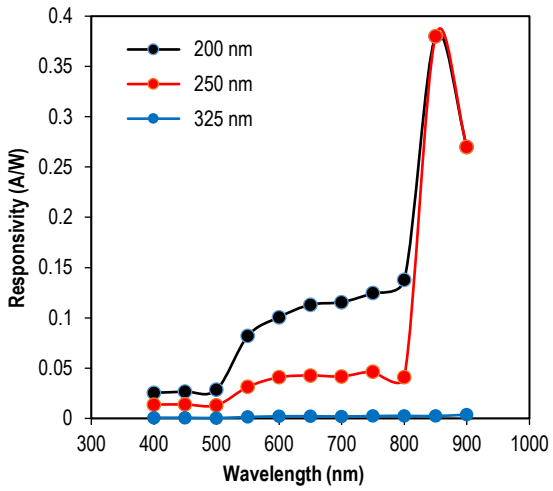

Fig. (3) The variation of spectral responsivity with wavelength for Al_2O_3/Si structures prepared with different thicknesses of Al_2O_3 layer (200, 250, and 325nm)

Figure (4) presents the external quantum efficiency (EQE) as a function of wavelength for the prepared Al_2O_3/Si structures. A clear trend in the magnitude and spectral distribution of EQE is observed with varying Al_2O_3 layer thickness. The first two samples (200 and 250 nm) exhibit remarkably similar EQE characteristics. Both show a relatively low EQE in the visible range (around 5-20%), but a significant increase in the near-infrared region, peaking at approximately 55-56% around 850 nm. This suggests that for this thickness range, the Al_2O_3 layer allows for efficient photon absorption in the silicon substrate at longer wavelengths. In contrast, the sample with 325nm Al_2O_3 layer thickness displays a drastically different and much lower EQE profile. The peak EQE for this sample is only about 0.52% (or 0.0052), which is orders of magnitude lower than the peaks observed in the first two samples. While it still shows some spectral dependence, the overall efficiency is severely diminished across the entire measured wavelength range. This substantial reduction in EQE for the thicker Al_2O_3 layer (325nm) indicates that while a thicker layer might improve insulation, it significantly hinders the generation and collection of photocarriers, likely due to increased optical absorption within the Al_2O_3 film itself, or a higher density of interface defects that act as recombination centers, thus severely limiting the device's performance as a photodetector.

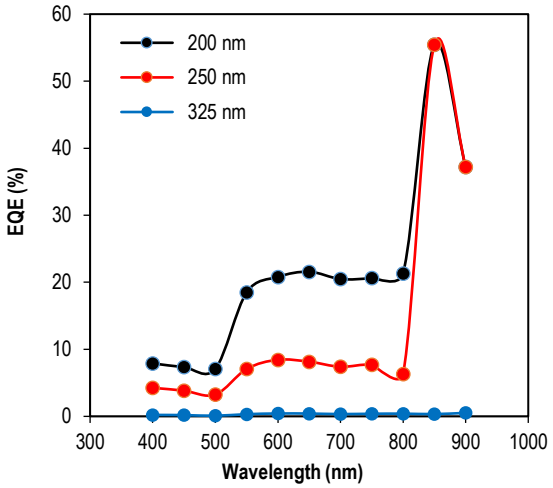

Fig. (4) The variation of EQE with wavelength for Al_2O_3/Si structures prepared with different thicknesses of Al_2O_3 layer (200, 250, and 325nm)

Figure (5) illustrates the specific detectivity (D^*) as a function of wavelength for the prepared Al_2O_3/Si structures. A clear and consistent trend in detectivity is observed across the samples, mirroring the previously discussed spectral responsivity. The first two samples (200 and 250 nm) exhibit very similar behaviors of detectivity, both showing relatively low values in the visible range and a sharp increase in the NIR region, peaking at approximately 0.55×10^{12} Jones around 850 nm. This indicates that for these deposition times, the Al_2O_3/Si structures are most sensitive to light in the NIR region, which is characteristic of silicon-based photodetectors. In stark contrast, the sample with 325nm Al_2O_3 layer thickness displays significantly lower detectivity values across the entire spectrum. The peak detectivity for this sample is only about 0.0055×10^{12} Jones, which is two orders of magnitude lower than the peaks observed in the first two samples. This substantial reduction in detectivity for the thicker Al_2O_3 layer (325nm) confirms that while a thicker layer might improve insulation, it severely degrades the overall signal-to-noise ratio (SNR) and thus the ability of the device to detect weak optical signals. This

suggests an optimal Al_2O_3 layer thickness exists for maximizing photodetection performance in these Al_2O_3/Si structures.

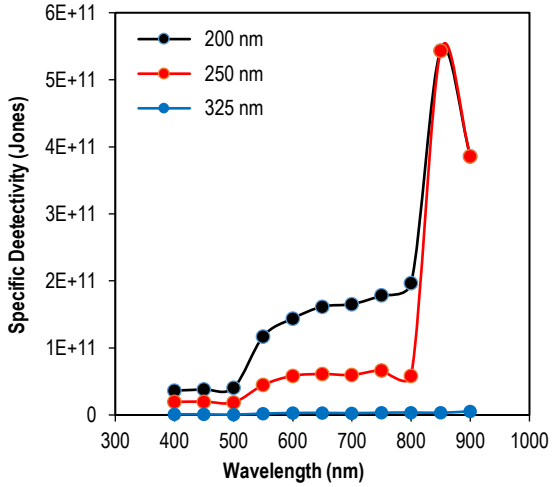

Fig. (5) The variation of specific detectivity with wavelength for Al_2O_3/Si structures prepared with different thicknesses of Al_2O_3 layer (200, 250, and 325nm)

4. Conclusion

The Al_2O_3 layer thickness is a critical factor dictating the electrical and optoelectronic performance of Al_2O_3/Si structures. Thicker Al_2O_3 layers (e.g., 325 nm) improve insulating properties by significantly reducing leakage current, however, they severely degrade photodetection capabilities, leading to diminished photocurrent, responsivity, external quantum efficiency, and detectivity. Conversely, an Al_2O_3 thickness in the 200-250 nm range appears optimal, offering a balanced performance with strong photoresponse, high NIR sensitivity (peaking around 800-850 nm), and superior specific detectivity, characteristic of efficient silicon-based photodetectors. This highlights a clear trade-off between insulation and light-detection efficiency.

References

[1] P.M. Martin, **"Introduction to Surface Engineering and Functionally Engineered Materials"**, Ch. 6, John Wiley & Sons (NJ, 2011), p. 339.

[2] A.S. Reddy, H.-H. Park and V.S. Reddy, "Effect of sputtering power on the physical properties of dc magnetron sputtered copper oxide thin films", *Mater. Chem. Phys.*, 110(2-3) (2008) 397-401.

[3] K. Seshan, **"Handbook of Thin Film Deposition: Techniques, Processes, and Technologies"**, 3rd ed., Ch. 4, William Andrew (Amsterdam, 2012).

[4] D. Mattox, **"Handbook of Physical Vapor Deposition (PVD) Processing"**, 2nd ed., Ch. 7, William Andrew, (Amsterdam, 2010).

[5] F.J. Kadhim et al., "Fabrication of UV Photodetector from Nickel Oxide Nanoparticles Deposited on Silicon Substrate by Closed-Field Unbalanced Dual Magnetron Sputtering Techniques", *Opt. Quantum Electron.*, 47(12) (2015) 3805-3813.

[6] D.A. Taher and M.A. Hameed, "Employment of Silicon Nitride Films Prepared by DC Reactive Sputtering Technique for Ion Release Applications", *Iraqi J. Phys.*, 21(3) (2023) 33-40.

[7] A. V. Tumarkin et al., "Preparation of alumina thin films by reactive modulated pulsed power magnetron sputtering with millisecond pulses", *Coatings*, 14(1) (2024) 82.

[8] M.K. Khalaf et al., "Fabrication and Characterization of UV Photodetectors Based on Silicon Nitride Nanostructures Prepared by Magnetron Sputtering", *Proc. IMechE, Part N, J. Nanomater. Nanoeng. Nanosys.*, 230(1) (2016) 32-36.

[9] C. Otero et al., "Optoelectronic Response of Multilayer CuO/NiO Nanostructures Fabricated with Different Particle Size Ranges", *Iraqi J. Appl. Phys. Lett.*, 8(1) (2025) 29-32.

[10] M.A. Hameed and Z.M. Jabbar, "Preparation and Characterization of Silicon Dioxide Nanostructures by DC Reactive Closed-Field Unbalanced Magnetron Sputtering", *Iraqi J. Appl. Phys.*, 12(4) (2016) 13-18.

[11] K.A. Aadim, "Control the deposition uniformity using ring cathode by DC discharge technique", *Iraqi J. Phys.*, 15(32) (2017) 57-60.

[12] G. Angarita et al., "Synthesis of alumina thin films using reactive magnetron sputtering method", *IOP Conf. Ser.: J. Phys.*, 850 (2017) 012022.

[13] G. Zhou et al., "Deposition of nanostructured crystalline alumina thin film by twin targets reactive high power impulse magnetron sputtering", *Appl. Surf. Sci.*, 455 (2018) 310-317.

[14] O.A. Hammadi, "Nanostructured CdSnSe Thin Films Prepared by DC Plasma Sputtering of Thermally Casted Targets", *Iraqi J. Appl. Phys.*, 14(4) (2018) 33-36.

[15] R.A. Anaee et al., "Alumina Nanoparticle/Polypyrrole Coating for Carbon Steel Protection in Simulated Soil Solution", *Eng. Tech. J.*, 35(9A) (2017) 943-949.

[16] M. Said et al., "Microwave hybrid heating for lead-free solder: A review", *J. Mater. Res. Technol.*, 26 (2023) 6220-6243.

[17] F.J. Al-Maliki et al., "Optimization of Rutile/Anatase Ratio in Titanium Dioxide Nanostructures prepared by DC Magnetron Sputtering Technique", *Iraqi J. Sci.*, 60(special issue) (2019) 91-98.

[18] M.K. Lambert et al., "Physical properties of γ–Al_2O_3 nanostructures prepared by high-

temperature casting", *Mater. Eng. Technol.*, 25(1) (2020) 33-42.
[19] B.K. Nasser and M.A. Hameed, "Structural Characteristics of Silicon Nitride Nanostructures Synthesized by DC Reactive Magnetron Sputtering", *Iraqi J. Appl. Phys.*, 15(4) (2019) 33-36.
[20] F.J. Al-Maliki and E.A. Al-Oubidy, "Effect of gas mixing ratio on structural characteristics of titanium dioxide nanostructures synthesized by DC reactive magnetron sputtering", *Physica B: Cond. Matter*, 555 (2019) 18-20
[21] S.H. Faisal and M.A. Hameed, "Heterojunction Solar Cell Based on Highly-Pure Nanopowders Prepared by DC Reactive Magnetron Sputtering", *Iraqi J. Appl. Phys.*, 16(3) (2020) 27-32.
[22] S.U. Ilyasa, R. Pendyalaa, and N. Marneni, "Stability and Agglomeration of Alumina Nanoparticles in Ethanol-Water Mixtures", *Procedia Eng.*, 148 (2016) 290-297.
[23] R.H. Turki and M.A. Hameed, "Spectral and Electrical Characteristics of Nanostructured NiO/TiO_2 Heterojunction Fabricated by DC Reactive Magnetron Sputtering", *Iraqi J. Appl. Phys.*, 16(3) (2020) 39-42.
[24] K.A. Al-Hamdani, "Current–voltage and capacitance-voltage characteristics of Se/Si heterojunction prepared by DC planar magnetron sputtering technique", *Iraqi J. Phys.*, 8(13) (2010) 97-100.
[25] N. Zaim and O. Bayhatun, "A Study on the Gamma-Ray Attenuation Coefficients of Al_2O_3 and Al_2O_3.TiO_2 Compounds", Süleyman Demirel University Journal of Natural and Applied Sciences, 22 (2018) 312-318.
[26] X. Zheng et al., "Microstructure and electrical contact behavior of Al2O3–Cu/30W3SiC(0.5Y2O3) composites", *J. Mater. Res. Technol.*, 22 (2023) 2158-2173.
[27] M.A. Hameed et al., "Characterization of Multilayer Highly-Pure Metal Oxide Structures Prepared by DC Reactive Magnetron Sputtering Technique", *Iraqi J. Appl. Phys.*, 16(4) (2020) 25-30
[28] Y. Zhang et al., "A review paper on effect of the welding process of ceramics and metals", *J. Mater. Res. Technol.*, 9(6) (2020) 16214-16236.
[29] A.N. Munif and F.J. Kadhim, "Structural Characteristics and Photocatalytic activity of TiO2/Si3N4 nanocomposite synthesized via plasma sputtering technique", *Iraqi J. Phys.*, 22(4) (2024) 99-106.
[30] E. Kianfar and V. Cao, "Polymeric membranes on base of PolyMethyl methacrylate for air separation: a review", *J. Mater. Res. Technol.*, 10 (2021) 1437-1461.
[31] N.A.H. Hashim and F.J. Kadhim, "Structural and Optical Characteristics of Co_3O_4 Nanostructures Prepared by DC Reactive Magnetron Sputtering", *Iraqi J. Appl. Phys.*, 18(4) (2022) 31-36.
[32] A.Y. Bahlool, "Temperature-Dependent Optoelectronic Characteristics of p-SnO_2/n-Si Heterojunction Structures", *Iraqi J. Appl. Phys. Lett.*, 7(1) (2024) 23-26.
[33] A.M. Hameed and M.A. Hameed, "Spectroscopic characteristics of highly pure metal oxide nanostructures prepared by DC reactive magnetron sputtering technique", *Emerg. Mater.*, 6 (2022) 627-633.
[34] D.A. Taher and M.A. Hameed, "Spectroscopic Characteristics of Silicon Nitride Thin Films Prepared by DC Reactive Sputtering Using Silicon targets with Different Types of Conductivity", *Iraqi J. Appl. Phys.*, 19(4A) (2023) 73-76.
[35] R. Darwesh et al., "Improved radiation shielding properties of epoxy resin composites using Sb_2O_3 and Al_2O_3 nanoparticles additives", *Annals Nucl. Ener.*, 200 (2024) 110385.
[36] M.S. Edan, "Copper Nitride Nanostructures Prepared by Reactive Plasma Sputtering Technique", *Iraqi J. Mater.*, 4(1) (2025) 31-36.
[37] D.A. Taher and M.A. Hameed, "Structural and Hardness Characteristics of Silicon Nitride Thin Films Deposited on Metallic Substrates by DC Reactive Sputtering Technique", *Silicon*, 15 (2023) 7855-7864.
[38] M.A. Hameed et al., "Characterization of Multilayer Highly-Pure Metal Oxide Structures Prepared by DC Reactive Magnetron Sputtering", *Iraqi J. Mater.*, 3(4) (2024) 1-8.
[39] M.K. Khalaf et al., "Operation Characteristics of a Closed-Field Unbalanced Dual-Magnetrons Plasma Sputtering System", *Bulg. J. Phys.*, 41(1) (2014) 24-33.
[40] M.A. Hameed and Z.M. Jabbar, "Optimization of Preparation Conditions to Control Structural Characteristics of Silicon Dioxide Nanostructures Prepared by Magnetron Plasma Sputtering", *Silicon*, 10(4) (2018) 1411-1418.
[41] E.A. Al-Oubidy and F.J. Al-Maliki, "Effect of Gas Mixing Ratio on Energy Band Gap of Mixed-Phase Titanium Dioxide Nanostructures Prepared by Reactive Magnetron Sputtering Technique", *Iraqi J. Appl. Phys.*, 14(4) (2018) 19-23.
[42] A.M. Hameed and M.A. Hameed, "Highly-Pure Nanostructured Metal Oxide Multilayer Structure Prepared by DC Reactive Magnetron Sputtering Technique", *Iraqi J. Appl. Phys.*, 18(4) (2022) 9-14.

